Am J Transl Res 2025;17(8):6028-6041
www.ajtr.org /ISSN:1943-8141/AJTR0161830

Original Article

Knockdown of TIM1 enhances platinum chemosensitivity and inhibits progression through the MAPK signaling pathway in gastric cancer

Congkai Zhang[1,2*], Chao Zhu[1*], Haoxuan Huang[3], Mengwei Liu[1], Kuai Yu[1], Aiping Le[1]

[1]Department of Transfusion Medicine, Key Laboratory of Jiangxi Province for Transfusion Medicine, The First Affiliated Hospital, Jiangxi Medical College, Nanchang University, Nanchang, Jiangxi, P. R. China; [2]Department of Oncology, Jingzhou Hospital Affiliated to Yangtze University, Jingzhou, Hubei, P. R. China; [3]Department of Urology, The Third Affiliated Hospital of Nanchang University, Nanchang, Jiangxi, P. R. China. [*]Equal contributors.

Received November 7, 2024; Accepted July 9, 2025; Epub August 15, 2025; Published August 30, 2025

Abstract: Objectives: The incidence of gastric cancer (GC) is increasing worldwide, and it ranks among the leading causes of cancer-related mortality. Platinum-based chemotherapeutic agents are commonly employed in the treatment of various solid tumors; however, the development of drug resistance remains a crucial barrier to effective treatment. T cell immunoglobulin and mucin domain 1 (TIM1) has been implicated in the initiation and progression of various tumors. Nevertheless, the influence of TIM1 on the efficacy of platinum-based chemotherapeutics and its biologic implications in GC have not been thoroughly investigated. Methods: This study utilized flow cytometry, cell counting kit-8 assays, and western blot to assess the role of TIM1 in modulating sensitivity to platinum drugs. High-throughput sequencing was employed to elucidate the potential mechanism of TIM1. Additionally, the effect of TIM1 on the biologic characteristics of GC was further investigated through clinical specimens, cells, and animals. Results: Knockdown of TIM1 enhanced the sensitivity of GC cells to platinum chemotherapeutic drugs. Furthermore, TIM1 expression was elevated in GC tissues, and high TIM1 expression predicted poor survival outcomes in GC patients. Knockdown of TIM1 inhibited the malignant behaviors of GC cells in vitro and in vivo. The mitogen-activated protein kinase (MAPK) signaling pathway may play a role in the regulatory effects of TIM1 on GC cells. Conclusions: Overall, TIM1 functions as an oncogene in GC. Knockdown of TIM1 enhances platinum chemosensitivity and inhibits its malignant behavior in GC through the MAPK signaling pathway. These findings reveal a molecular mechanism contributing to chemotherapy resistance and suggest a therapeutic strategy for enhancing chemotherapy.

Keywords: Gastric cancer, T cell immunoglobulin and mucin domain 1, chemosensitivity, MAPK signaling pathway

Introduction

Gastric cancer (GC) is widely recognized, and the fourth most prevalent cancer worldwide [1]. Surgical resection is generally regarded as the standard and most effective treatment for early-stage GC patients; however, many patients are diagnosed at an advanced stage [2]. Despite the utilization of various treatment modalities, including surgical resection, chemotherapy, radiotherapy, targeted therapy, immunotherapy, and combination therapy, the 5-year overall survival rate for individuals with advanced GC is only 5%-20%, with a median overall survival time of approximately 10 months. This poor prognosis is largely attributable to the aggressive nature and high metastatic potential of advanced GC [3, 4].

Platinum-based chemotherapeutic agents are currently among the most effective treatments available for GC and are frequently administered either as monotherapies or in conjunction with other therapeutic agents [5]. These platinum compounds form intra-strand and inter-strand DNA-platinum adducts that inhibit gene transcription and can lead to G2/M phase cell cycle arrest by sequestering transcription factors [6]. Nonetheless, the emergence of primary and acquired resistance to platinum agents poses a significant obstacle to antitumor therapy [7]. The mechanisms underlying tumor resis-

https://doi.org/10.62347/VAFF5386

tance to platinum drugs are multifaceted, encompassing factors such as drug uptake, DNA damage repair mechanisms, apoptosis, and the modulation of autophagic copper transporters [8]. Xu *et al*. reported that the chemosensitivity to cisplatin can be enhanced through the depletion of intracellular glutathione (GSH) [9]. Furthermore, the mitogen-activated protein kinase (MAPK) signaling pathway, especially the classical extracellular regulated protein kinases 1/2 (ERK1/2) signaling pathway, is critical in determining sensitivity to platinum-based drugs [10, 11]. Therefore, it is imperative to develop strategies that effectively reverse or mitigate chemotherapy resistance, improve the efficacy of chemotherapeutic regimens, and ultimately enhance patient outcome.

T cell immunoglobulin and mucin domain 1 (TIM1), also referred to as kidney injury molecule 1 and hepatitis A virus cellular receptor 1 (HAVCR1), is recognized as a crucial susceptibility gene [12]. TIM1 was initially identified in African green monkeys and humans as a cellular receptor for hepatitis A virus [13]. As a vital costimulatory molecule on the surface of T cells, TIM1 expression has been observed to be elevated in human glioma tissues compared to normal tissues at the mRNA and protein levels. Notably, high levels of TIM1 expression have been associated with a poorer patient prognosis [14]. Momoko Nishikori *et al*. reported that primary central nervous system lymphoma (PCNSL) is characterized by TIM1 expression and that soluble TIM1 in the cerebrospinal fluid may serve as a valuable biomarker for PCNSL [15]. Alternatively, TIM1 may be a novel prognostic factor and therapeutic target for non-small cell lung cancer (NSCLC) [16]. These findings imply that TIM1 may function as an oncogene with a possible connection to tumorigenesis. In gastric cancer, Liu *et al*. were the first to report that HAVCR1 expression could serve as a novel prognostic factor [17]. A subsequent study indicated that HAVCR1 might influence GC tumor progression and patient outcomes. However, the carcinogenic effects and specific mechanisms by which TIM1 operates in GC remain unclear [18].

The objective of this study was to explore the biologic role and mechanisms of TIM1 in GC. Our findings indicate that inhibition of TIM1 can enhance GC cell sensitivity to platinum-based chemotherapeutic drugs. Furthermore, high-throughput sequencing suggested that the MAPK signaling pathway may be involved in TIM1 regulation on GC cells. We subsequently assessed the expression of TIM1 in GC and further studied its prognostic value and clinical significance. Additionally, both *in vitro* and *in vivo* experiments verified the influence of TIM1 on the malignant biologic behavior of GC. Overall, this study underscores the potential of TIM1 as a significant biomarker and a promising therapeutic target in GC.

Materials and methods

Cell culture

Human gastric mucosal epithelial cells (GES-1), human gastric cancer cell lines (BGC-823, SGC-7901, MGC-803, MKN-45, SNU-16), HGC-27 (human gastric cancer cells, undifferentiated), and human renal epithelial lines (HEK-293T) were originally acquired from the American Type Culture Collection (ATCC, Manassas, USA) and cultured as per instructions.

Plasmid and lentivirus transfection assay

The shNC and shTIM1 primers (sh1 and sh2) were designed by Shanghai Sangon Biotech (Shanghai, China), and shNC and TIM1 knockdown plasmids were constructed, respectively. The plasmid used to overexpress TIM1 was acquired from a public library of proteins and plasmids (Nanjing, China). The constructed plasmids underwent verification by agarose gel electrophoresis and DNA sequencing. HEK-293T cells were transfected with the above plasmids using Lipofectamine™ 2000 (Invitrogen, USA), producing a lentiviral vector that was then transduced into MGC-803 and MKN-45 GC cells. After 7 days of puromycin selection, the stable cell lines were harvested, and the transfection efficiency was further assessed by quantitative reverse transcription polymerase chain reaction (qRT-PCR) and western blot (WB). Stably transfected cells were collected for the following assays.

shNC-F: 5'-GATCCCGTCAGTATCGGCGGAATTCC-TCGAGGAATTCCGCCGATACTGACGGTTTT-TG-3', shNC-R: 5'-AATTCAAAAACCGTCAGTATC-GGCGGAATTCCTCGAGGAATTCCGCCGATAC-TGACGG-3', sh1-F: 5'-GATCGCCTTTGGAATAACA-ATCAAACTCGAGTTTGATTGTTATTCCAAAGGC-

TTTTTG-3', sh1-R: 5'-AATTCAAAAAGCCTTTGGAATAACAATCAAACTCGAGTTTGATTGTTATTCCAAAGGC-3', sh2-F: 5'-GATCGTGCAGAAGACTGAACAGACATCTCGAGATGTCTGTTCAGTCTTCTGCATTTTTG-3', sh2-R: 5'-AATTCAAAAATGCAGAAGACTGAACAGACATCTCGAGATGTCTGTTCAGTCTTCTGCAC-3'.

Cell proliferation assay

We inoculated logarithmic phase cells into 96-well plates (1×10^3 cells/well) and cultivated them for 0 h, 24 h, 48 h, and 72 h, respectively. At each designated time, Cell counting kit-8 (CCK-8) solutions (Beyotime, China) were introduced into per well. After cultivation for 2 h in the incubator, the optical density (OD) value at 450 nm was determined using a microplate reader.

Clone formation assay

Cells were implanted in 6-well plates (5×10^2 cells/well) and further cultivated for a duration of 14-21 days. Upon the emergence of visible clones within the wells, the clones were fixed with 4% paraformaldehyde solution and stained with crystal violet (CV) solution (Solarbio, China). Following this, the clones were washed, dried, and photographed with a microscope (Olympus, Japan). The proliferative potential of individual cells was evaluated by the calculation of the clone formation rate.

Scratch assay

An applicable density to scratch assay was established in 6-well plates. Consistent scratches were generated with pipette tips. After rinsing to clean the debris with phosphate buffer saline (PBS), the medium was renewed with a serum-free formulation devoid of fetal bovine serum (FBS). The cells were maintained in a cell incubator and photographed at predetermined times (0 h and 48 h). Cell migration was quantified by detecting the distance between the scratches by Image J software (National Institutes of Health).

Invasion assay

Cell invasion was assessed using a BD transwell chamber (6-well plates). In the matrigel-pretreated apical chambers pre-treated with matrigel, cells were inoculated with serum-free conditions. Then, 20% FBS was added into the basolateral compartment of the medium. After 24 h incubation, the remaining medium was removed, and the cells were further fixed at room temperature (RT). Subsequently, cells were washed with PBS, dyed with CV solution (Solarbio, China), and then visualized, photographed, and analyzed under a microscope.

Cell cycle assay

Briefly, the resuspended samples were fixed overnight in 70% ethanol at 4°C. Additionally, the cells were incubated at RT for 15 min with PBS buffer containing RNase, Triton X-100, and propidium iodide (PI). The distribution of the cell cycle was ultimately assessed using flow cytometry (Navios, Beckman Coulter, US).

Apoptosis assay

In 6-well plates, a similar number of GC cells were administered with either cisplatin or oxaliplatin for 24 h. Harvesting cells at a specific time, a 100 μL binding buffer was then employed to resuspend the cells. According to established protocols, annexin V and PI were applied to dye the samples in the dark at RT. The rate of apoptosis was quantified by flow cytometry (Navios, Beckman Coulter, US).

Western blot (WB)

Total cells were gathered and lysed with radio immunoprecipitation assay lysis buffer (Thermo Fisher Scientific, USA) supplemented with phenylmethylsulfonyl fluorid and phosphatase inhibitors (MedChemExpresson, USA), and maintained on ice for 30 min. The reactant was centrifuged (15000 × g, 10 min) to eliminate cell debris, and the protein concentration was subsequently quantified using the bicinchoninic acid assay protein kit (Beyotime, China). Equal quantities of protein were subjected to 10% sodium dodecyl sulfate-polyacrylamide gel electrophoresis, which were further shifted to the polyvinylidene fluoride membrane (Merck Millipore, USA). The membrane was blocked with 5% skim milk in tris buffered saline tween and incubated overnight at 4°C with specific primary antibodies, including TIM1 antibody (Abcam, USA), Na/K ATPase antibody (Abcam, USA), β-Actin antibody (Abcam, USA), Bax/Bcl-2 antibody (Abcam, USA), ERK1/p-ERK1 antibody (CST, USA), and p38/p-p38 antibody (CST, USA).

After multiple washes with PBS, the above membrane was incubated with horseradish peroxidase (HRP)-conjugated secondary antibody (RT, 1 h). A Chemiluminescence Kit (Millipore, MA, USA) was utilized to detect the target band, which was visualized by a gel imaging analysis system (Bio-Rad, USA). The target protein expression was quantified using ImageJ software.

Total RNA extraction and qRT-PCR

Total RNA was conventionally extracted from cells and tissues utilizing the conventional Trizol reagent (Invitrogen, USA), and further analyzed with a nanodrop 2000 spectrophotometer (Thermo Fisher Scientific, USA). Then, cDNA was synthesized by a reverse transcription kit (Promega, USA). According to the manufacturer's guidelines, qRT-PCR was executed with a detection system (Roche, Sweden). The relative expression of gene in each group was determined by the $2^{-\Delta\Delta Ct}$ method. The primer sequence of this research is displayed, with GAPDH employed as the internal control. All primers were sourced from Sangon Biotech (Sangon, China).

RNA sequencing (RNA-seq) analysis

RNA-seq analyses were conducted by HaploX Biotechnology (Shenzhen, China). The transcriptome correlation analysis was performed as follows: total RNA was extracted from cell samples across each group, and quality evaluation was performed as previously described. The sample library was constructed and sequencing was executed in accordance with Illumina's standard protocol. Thereafter, the analysis of differential genes between samples or groups was based on quantitative gene expression data. Differentially expressed genes (DEGs) were recognized with the criteria of $|\log_2(\text{FoldChange})| > 1$ and $p.\text{adj} < 0.05$. The volcano plot and heat map were generated by R packages. Finally, the identified DEGs were subjected to Kyoto Encyclopedia of Genes and Genomes (KEGG) functional enrichment analysis.

Animal experiments

Four-week-old female BALB/c nude mice (n = 18) were acquired from Hangzhou Ziyuan Experimental Animal Co., Ltd. (Hangzhou, China) which were assigned to the shNC group, Sh2 group, and Sh2 + $TIM1^{RES}$ group (n = 6 per group) at random. They were maintained under a specific pathogen free environment, suitable temperature, and humidity with a standard diet. MGC-803 cells, which had been infected with shRNA, Sh2, and Sh2 + $TIM1^{RES}$ lentivirus (5×10^6 cells, 0.2 mL PBS) were inoculated into the right axillary region of nude mice in the shNC group, Sh2 group, and Sh2 + $TIM1^{RES}$ group, respectively. The tumor diameters were recorded every 5 days for 3 consecutive weeks. Tumor volume was subsequently evaluated by the measurements of tumor length and short axis diameter. Thereafter, the mice were sacrificed and the tumors were resected to calculate the volume and weight. Meanwhile, a portion of the tumors were kept at -80°C for the following qRT-PCR assay, and the others were fixed for staining (Ki-67 antibody, Abcam, USA). All animal experiments were approved by the Experimental Animal Welfare Ethics Committee of the First Affiliated Hospital of Nanchang University and were carried out in accordance with the criteria and procedures for animal care and welfare.

Immunohistochemistry (IHC) staining

The cancer tissues and paracancerous tissues were procured from the First Affiliated Hospital of Nanchang University with the patient's written consent and approved by Ethics Committee of the First Affiliated Hospital of Nanchang University. After all the tissues were sufficiently fixed under 4% paraformaldehyde, the specimens underwent overnight dehydration and were subsequently embedded with paraffin. Then the tissues were sectioned to slices of appropriate thickness, and a series of processes were carried out involving deparaffinization, rehydration, microwave-assisted antigen retrieval, deactivation of endogenous peroxidase with a hydrogen peroxide solution, and serum blocking. After that, the rabbit pAb against TIM1 (Abcam, USA) was applied to slides and incubated overnight at 4°C away from light, followed by incubation with the HRP-conjugated secondary antibody (Abcam, USA) at RT for 1 h. Subsequently, the slices were further counterstained under diaminobenzidine and Hematoxylin and eosin (H&E). Each slide was independently assessed by two qualified

pathologists under a microscope and yellow, brown yellow, or brown granules were considered as positive cells.

Statistical analysis

The data were shown as mean ± standard deviation (SD) and were processed by GraphPad Prism 9 software (GraphPad InStat Software, CA, USA) and SPSS software (version 23.0). Each experiment should be repeated three times. The Student's t-test (two-tailed) was employed to assess the differences between two groups, whereas one-way analysis of variance (ANOVA) was utilized to evaluate the differences among multiple groups. $*P < 0.05$, $**P < 0.01$, $***P < 0.001$, $****P < 0.0001$, and ns (no significant).

Results

Knockdown of TIM1 enhanced the sensitivity of GC cells to platinum drugs

Platinum-based chemotherapeutic agents are the primary treatment for GC; however, platinum resistance remains a substantial challenge [6, 19]. A search of the Genomics of Drug Sensitivity in Cancer database revealed that the half maximal inhibitory concentration (IC_{50}) of the platinum drug cisplatin correlated positively with TIM1 expression in GC cell lines Figure S1. To further investigate TIM1 expression, qRT-PCR and WB were employed to assess TIM1 expression in normal gastric epithelial cells (GES-1) and several GC cell lines, including BGC-823, SGC-7901, MGC-803, MKN-45, SNU-16, and HGC-27. The findings revealed that TIM1 was highly expressed in the above GC cell lines, especially in MGC-803 and MKN-45 cells compared to that of GES-1 cells Figure S2A, S2B. Consequently, MGC-803 and MKN-45 cells were selected for subsequent experimental analysis. In addition, two shRNAs, designated as sh1 and sh2, resulted in high TIM1 knockdown efficiency in both MGC-803 and MKN-45 cells Figure S3A, S3B. Next, TIM1 was overexpressed in these cells via sh2, resulting in the designation of $TIM1^{RES}$ Figure S3A, S3B.

Cell apoptosis was evaluated by flow cytometry to investigate the effect of TIM1 expression levels on the sensitivity of GC cells to platinum-based drugs. Among the MGC-803 cells, the percentages of total apoptotic cells in the shNC, sh1, and sh2 groups were 3.0%, 9.5%, and 12.5%, respectively. In contrast, the percentage of apoptotic cells was reduced to 5.7% after the overexpression of TIM1 (**Figure 1A**, **1B**). Similarly, in MKN-45 cells, the downregulation of TIM1 expression increased cell apoptosis, and its upregulation in the sh2 + $TIM1^{RES}$ group inhibited apoptosis to a certain extent (**Figure 1A**, **1B**). MGC-803 and MKN-45 cells were subsequently subjected to treatment with platinum-based agents. The proportion of apoptotic cells in each group was increased with increasing drug concentration. In detail, upon 1 μg/mL cisplatin treatment, the total percentages of apoptotic MGC-803 cells in the sh1 and sh2 groups were 24.2% and 25.0%, respectively (**Figures 1C**, S4A). In contrast, the apoptotic rate was only 11.0% in the shNC group, while it increased to 19.7% in the sh2 + $TIM1^{RES}$ group. By increasing cisplatin concentration to 5 μg/mL, the apoptotic rates were up to 58.2% and 74.4% in the sh1 and sh2 groups, respectively. In contrast, the apoptotic rate was just 29.4% in the shNC group and 45.7% in the sh2 + $TIM1^{RES}$ group (**Figures 1C**, S4A). Similarly, after 1 μg/mL cisplatin treatment, the apoptotic rates of MKN-45 in the sh1 and sh2 groups were 19.3% and 24.5% respectively Figure S5A, S5B. Conversely, the apoptotic rate was a mere 12.9% in the shNC group and 15.7% in the sh2 + $TIM1^{RES}$ group. Raising cisplatin concentration to 5 μg/mL, the apoptotic rates observed in the sh1 and sh2 groups were 53.3% and 76.9%, in contrast to 34.6% in the shNC group and 44.0% in the sh2 + $TIM1^{RES}$ group Figure S5A, S5B. The same tendency was also noted after oxaliplatin treatment (**Figures 1D**, S4B, S5C, S5D). Additionally, following exposure to platinum drugs, the cell viability of MGC-803 and MKN-45 cells across all groups exhibited a concentration-dependent decline, especially in the sh1 and sh2 groups (**Figures 1E**, **1F**, S5E, S5F). However, up-regulation of TIM1 appeared to mitigate the trend to a certain extent.

The Bcl-2 and Bax genes are integral to the regulation of apoptosis, and the reduction of the Bcl-2/Bax ratio is associated with the promotion of apoptosis in tumor cells [20, 21]. Here, we assessed the expression of Bcl-2 and Bax proteins by WB assay. The results displayed that the expression level of Bax was notably

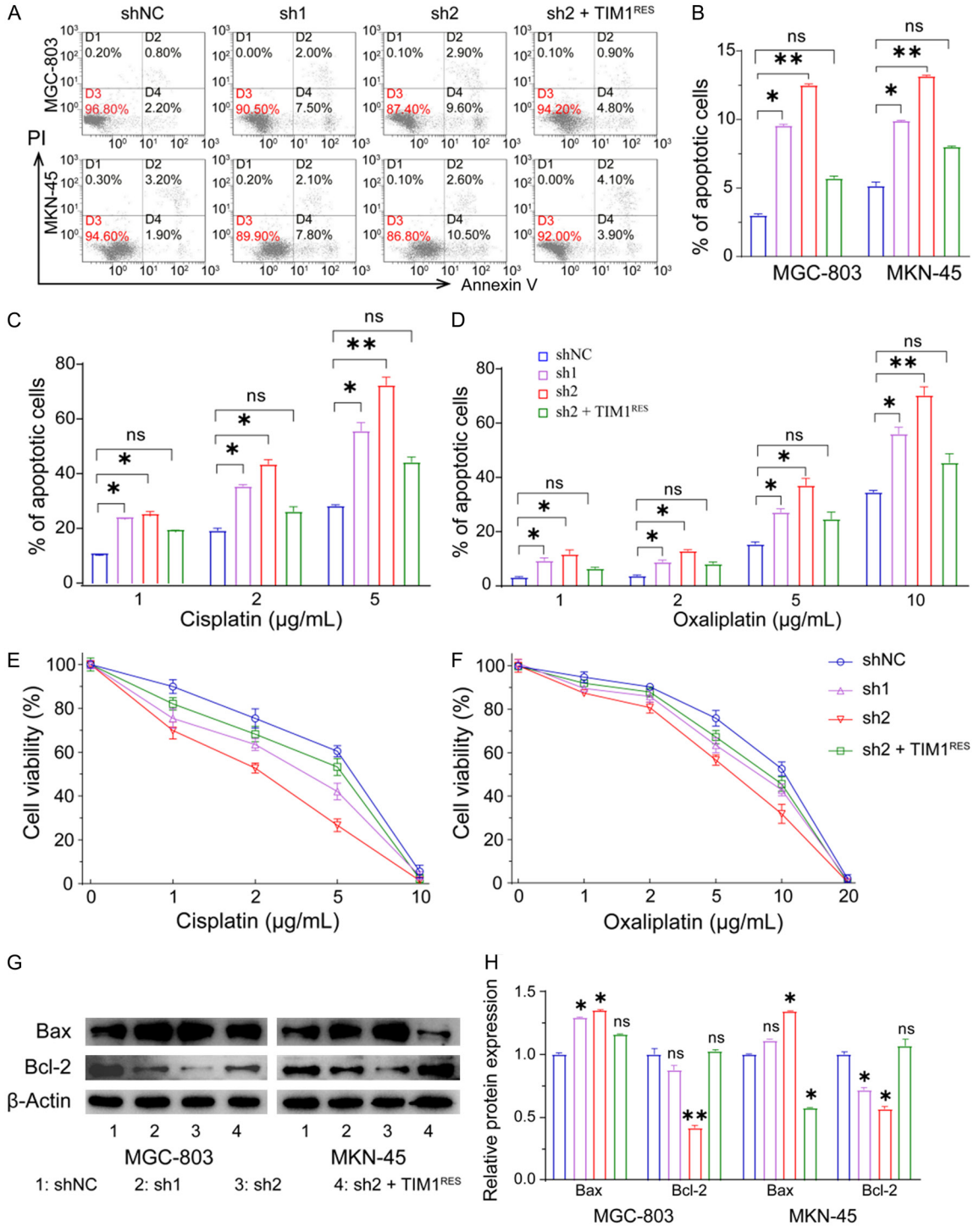

Figure 1. Knockdown of T cell immunoglobulin and mucin domain 1 (TIM1) enhanced the sensitivity of gastric cancer (GC) cells to platinum chemotherapeutic drugs. (A) Cell apoptosis was detected by staining with Annexin V and propidium iodide (PI) after shNC, TIM1 knockdown (sh1 and sh2), and TIM1 overexpression ($TIM1^{RES}$) in MGC-803 cells and MKN-45 cells. (B) Histograms of the results from each group of apoptotic cells are shown in (B). (C, D) After 48 h of treatment with different concentrations of cisplatin (C) and oxaliplatin (D), the histograms of the corresponding apoptosis of MGC-803 cells in each group. (E, F) After 48 h of treatment with different concentrations of cisplatin (E) and oxaliplatin (F), the cell viability of MGC-803 cells was assessed by cell counting kit-8 (CCK-8) assay. (G) The protein levels of Bax and Bcl-2 were determined by western blot (WB) assay (β-Actin: internal control). (H) Quantification of Bax and Bcl-2. Data are shown as mean ± standard deviation (SD). $*P < 0.05$, $**P < 0.01$, and ns (no significant).

increased in the TIM1 knockdown (sh1 and sh2) groups, while expression was suppressed in the sh2 + $TIM1^{RES}$ group (**Figure 1G**, **1H**). Conversely, Bcl-2 levels exhibited an inverse pattern, which was consistent with the above results of apoptosis and cell viability assays. Together, these findings suggest that the inhibition of TIM1 can enhance the sensitivity of GC cells to platinum-based drugs.

Exploring the mechanism of TIM1 in GC

To elucidate the potential mechanism of TIM1 in GC, mRNA sequencing (RNA-seq) and bioinformatic analyses were conducted on MGC-803 from both the shNC and sh2 groups. In **Figure 2A**, the results of the volcano map show that 928 genes were up-regulated, and 563 genes were down-regulated in the sh2 group compared to the shNC group (red represents the genes with up-regulation, and green represents the genes with down-regulation). Afterward, GO and KEGG enrichment analyses were performed to explore the signaling pathways influenced by TIM1 (**Figure 2B**, **2C**). The GO enrichment analysis encompassed molecular function (MF), cellular composition (CC), and biological process (BP). Specifically, the results of the MF enrichment analysis highlighted a dramatic enrichment of MAPK kinase tyrosine/serine/threonine phosphatase activity (**Figure 2B**). Concurrently, the BP enrichment analysis revealed substantial enrichment in the stress-activated MAPK cascade and regulation of cell cycle phase transition. Moreover, KEGG enrichment analysis identified pathways that were notably enriched including the MAPK signaling pathway, interleukin-17 (IL-17) signaling pathway, and the janus kinase signal transducer and activator of transcription (JAK-STAT) signaling pathway, all of which are associated with tumor development and progression (**Figure 2C**). In particular, the number of DEGs enriched in the MAPK signaling pathway was both maximal and conspicuous.

The MAPK signaling pathway exerts a crucial role in tumor genesis and progression [22, 23], and it is also closely associated with resistance against chemotherapy agents such as oxaliplatin and 5-Fluorouracil (5-FU) [24]. Through WB assay, we verified whether TIM1 exerted efficacy by the MAPK signaling pathway. We found that the levels of ERK1 were comparable across all groups, while the levels of p-ERK1 and p-ERK1/ERK1 were rmarkedly reduced in the TIM1 knockdown group and elevated in the sh2 + $TIM1^{RES}$ group (**Figure 2D-F**). Additionally, the p-p38/p38 also revealed analogous trends. These findings corroborated the results obtained from the mRNA-seq analysis. In conclusion, TIM1 may exert its effects through the MAPK signaling pathway in GC cells.

High TIM1 expression predicted poor survival of GC patients

Based on http://gepia.cancer-pku.cn, the expression levels of TIM1 in GC tissues were elevated compared to those of non-tumor tissues (**Figure 3A**). The increased expression of TIM1 was correlated with a poor prognosis of GC patients (**Figure 3B**). A similar phenomenon was observed in the TCGA and GSE62254 databases Figure S6. Additionally, the expression of TIM1 in both GC tissues and paracancer tissues was detected by IHC staining, and a representative picture in **Figure 3C** indicates that TIM1 expression is upregulated in GC. The samples were categorized into high and low TIM1 expression groups by the IHC score based on the median TIM1 values. Furthermore, Kaplan-Meier analysis, accompanied by the log-rank test, revealed that the overall survival of the GC patients exhibiting high TIM1 expression was distinctly lower than that of GC patients with low TIM1 expression ($P = 0.006$, **Figure 3D**). Taken together, TIM1 expression is inversely correlated with the prognosis in GC patients.

Knockdown of TIM1 inhibited the malignant biologic behaviors of GC cells in vitro

The study further explored the function of TIM1 in the malignant biologic behavior of GC cells. The CCK-8 assay indicated that knockdown of TIM1 distinctly reduced the proliferation of cells (MGC-803 and MKN-45), whereas up-regulation of TIM1 exerted the opposite effect (**Figure 4A**, **4B**). Additionally, the Clone formation assay suggested that clone formation ability to form clones diminished with TIM1 inhibition; nevertheless, TIM1 overexpression enhanced this ability (**Figure 4C**, **4D**). Furthermore, by scratch assay and transwell invasion, it was examined that knockdown of TIM1 substantially inhibited the metastasis and invasion of cells, in contrast to TIM1 overexpression, which facilitated these processes (**Figures 4E-H**, S7A-D). Next,

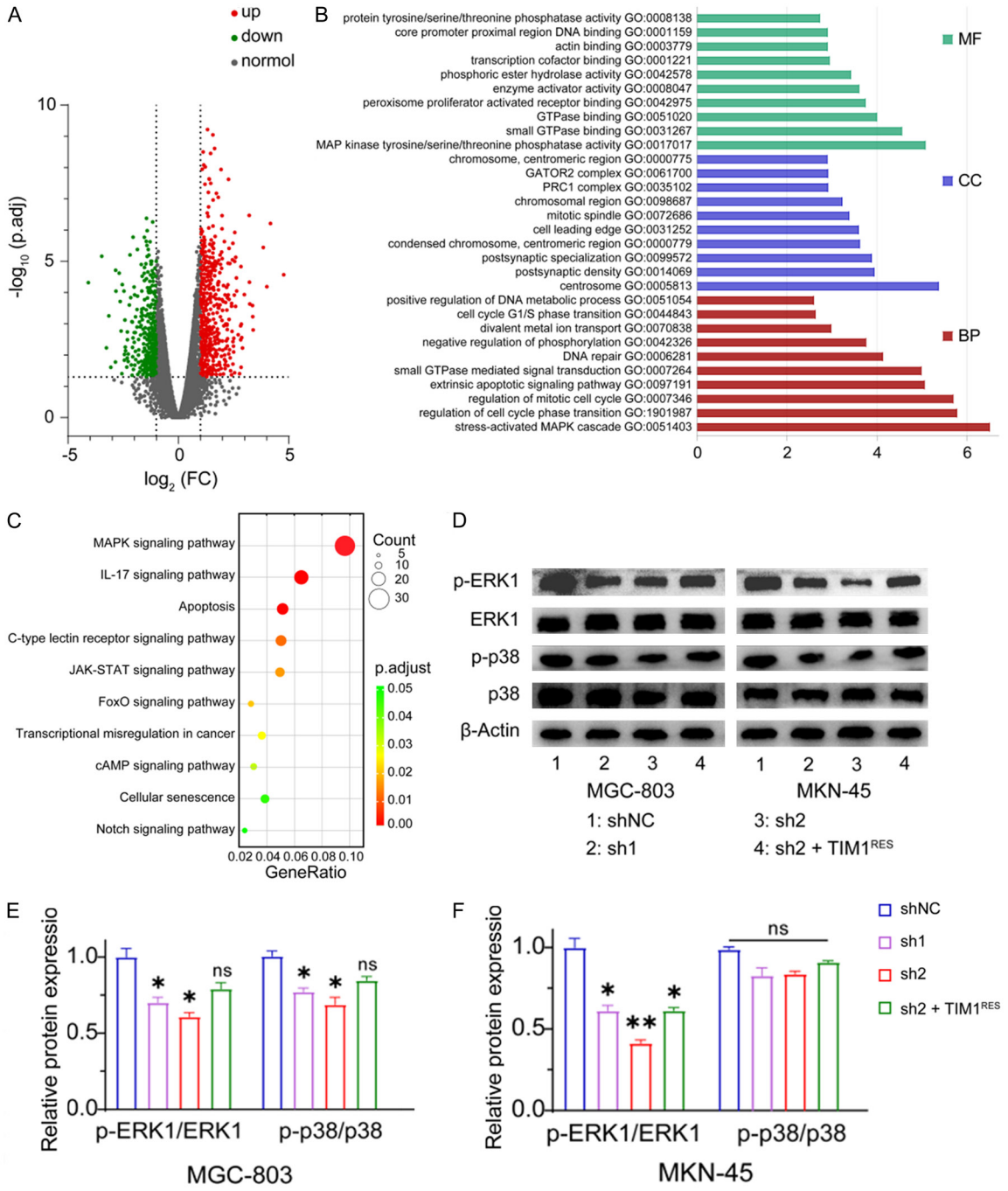

Figure 2. Potential mechanism of TIM1 regulating GC cells. The shNC group and sh2 group in MGC-803 GC cells were analyzed by RNA-seq. A. Volcano plots verified the up-regulated and down-regulated genes. Red: the up-regulated, green: the down-regulated, grey: normal, $\log_2$ (FC): $\log_2$ (FoldChange). B. The GO functional enrichment analysis of differentially expressed genes (DEGs). MF: molecular function, CC: cell composition, BP: biological process. C. The Kyoto Encyclopedia of Genes and Genomes (KEGG) pathway functional enrichment analysis of DEGs. D. The protein levels of ERK1, p-ERK1, p38, and p-p38 were determined by WB assay (β-Actin: internal control). E, F. Quantification of p-ERK1/ERK1, and p-p38/p38. Data were shown as mean ± SD. *P < 0.05, **P < 0.01, and ns.

the cell cycle detection also manifested that down-regulation of TIM1 upgraded the proportion of G1-phase cells, while upregulation of TIM1 reversed this phenomenon (**Figures 4I**, **4J**, S7E, S7F). In summary, down-regulation of TIM1 appears to inhibit the malignant charac-

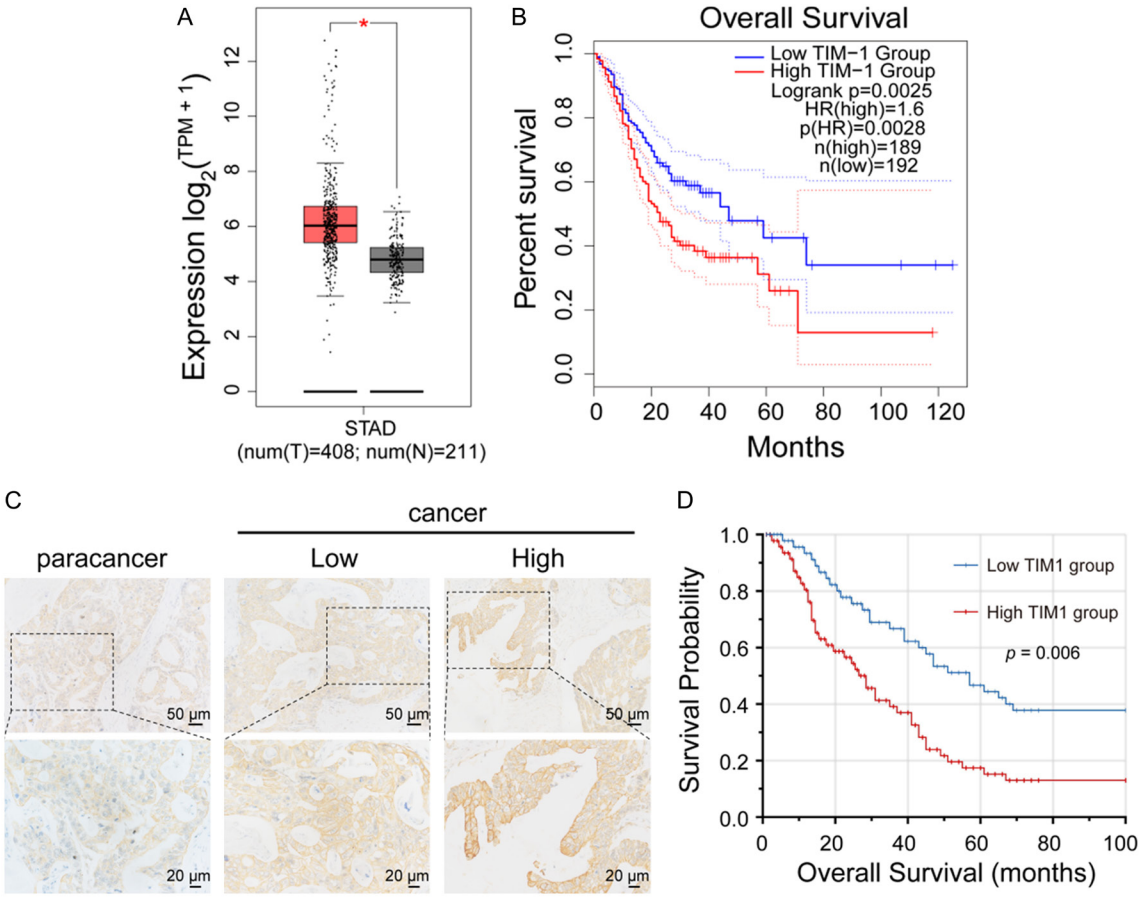

Figure 3. TIM1 was upregulated in GC and high TIM1 expression predicted poor survival of GC patients. A. The expression of TIM1 in tumor tissues and nontumor tissues from the TCGA database. B. The overall survival curve between patients expressing high-TIM1 and low-TIM1 was obtained by Kaplan-Meier survival analysis in the TCGA database. C. Representative pictures of TIM1 expression level in different groups. D. The TIM1 expression level was significantly correlated with overall survival.

teristics of GC cells by repressing proliferation, invasion, and migration, as well as inducing cell cycle arrest.

Knockdown of TIM1 repressed the growth of GC cells in vivo

To further determine the effect of TIM1 on GC growth *in vivo,* we established three stably transfected MGC-803 cell lines, designated as shNC, sh2, and sh2 + TIM1^{RES}, respectively. These cell lines were subsequently inoculated the cells into the right armpit tissue of immunodeficient mice. The growth of subcutaneous tumors (both the volumes and weights) were remarkably slower in the sh2 group than in the shNC group. Whereas the growth capacity was partially restored in the sh2 + TIM1^{RES} group (**Figure 5A-C**). Then, the H&E and IHC staining were performed. The cells represented a more normal morphology in the sh2 group (**Figure 5D**). As a nuclear antigen related to cell proliferation, the expression intensity of Ki-67 can determine the proliferative rate of tumors [25]. IHC staining presented a marked decrease in the number of Ki-67 positive cells in the sh2 group (**Figure 5E**). In short, the depletion of TIM1 was found to suppress the growth of GC cells *in vivo.*

Discussion

Gasrtric cancer (GC) is prevalent and has a poor prognosis despite advancements in clinical diagnosis and treatment [26]. Numerous studies have revealed that GC is highly susceptible to metastasis, recurrence, and resistance to chemotherapy, all of which are closely linked to its biologic characteristics [27]. The pathogenesis of GC is particularly complex; however,

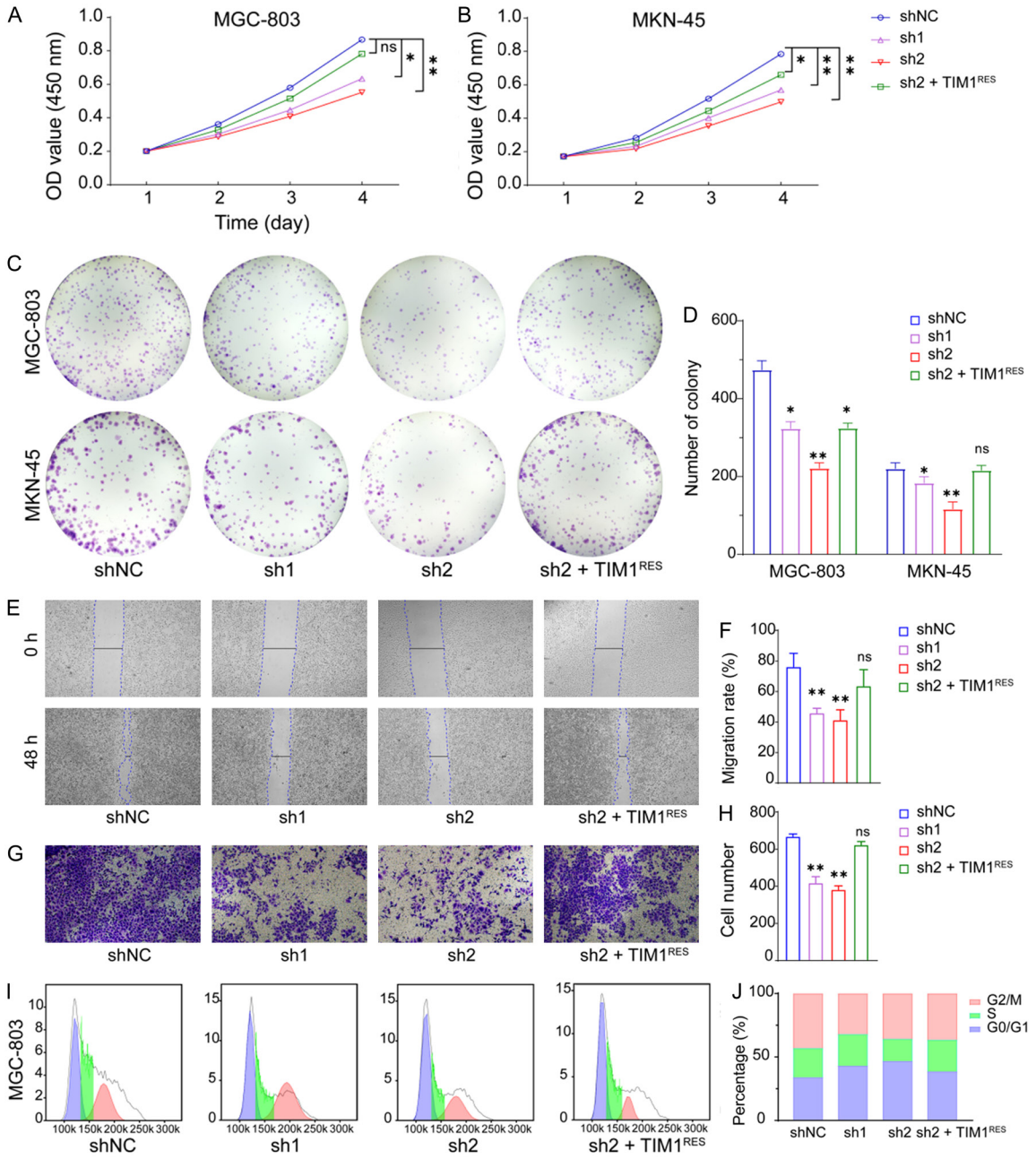

Figure 4. Knockdown of TIM1 inhibited the malignant biological behavior of GC cells *in vitro*. (A, B) Cell growth of MGC-803 (A) and MKN-45 (B) cells with shNC, TIM1 knockdown, and TIM1^{RES} assessed by CCK8 assay. (C, D) Colony formation assay and quantification of the number of shNC, TIM1 knockdown, and TIM1^{RES} in MGC-803 and MKN-45 cells. (E) Cell migration ability of MGC-803 cells with shNC, TIM1 knockdown, and TIM1^{RES} detected by scratch assay. (F) Bar graphs showed the percentage of migration rate in each group. (G, H) Representative images of trans-well invasion assay in each group of MGC-803 cells (G) and quantification of the number of invaded cells in each group (H). (I) Flow cytometry was performed to detect the cell cycle of MGC-803 in each group (left). (J) The percentages of MGC-803 cells in the different cycle phases are shown on the right. Data are shown as mean ± SD. *P < 0.05, **P < 0.01, and ns.

an increasing number of genes correlated with its onset are gradually being identified [28]. There is an urgent need to further investigate the molecular mechanisms underlying GC [29, 30]. Consequently, the identification of molecular markers closely associated with the pathogenic mechanisms of GC, followed by the development of targeted therapies, holds significant

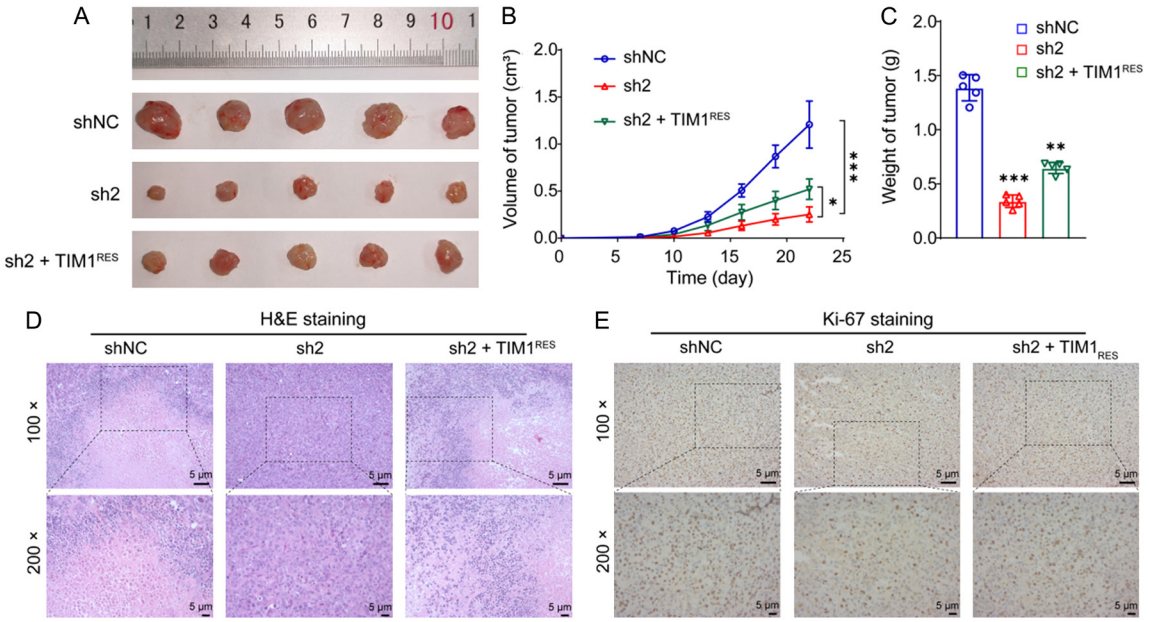

Figure 5. TIM1 knockdown repressed the growth of GC cells *in vivo*. A. Representative photos in each group of xenograft tumors. B. Tumor growth in nude mice was assessed by caliper at the indicated time intervals. C. The weight of tumors. D. Representative images of H&E staining in each group of xenograft tumors. E. Representative images of Immunohistochemistry (IHC) staining for Ki67 in each group. Data are shown as mean ± SD. **P* < 0.05, ***P* < 0.01, AND ****P* < 0.001.

promise for enhancing the prevention and treatment of GC.

Platinum-based agents represent a primary class of therapeutic agents utilized in GC, demonstrating significant efficacy in increasing patient survival rates [5]. However, the emergence of resistance to these agents remains a predominant factor contributing to treatment failure [6]. TIM1, a pivotal member of the TIM family, is considered a vital co-stimulatory molecule, and it has garnered considerable attention for its involvement in oncogenesis [31]. This study revealed that knockdown of TIM1 could enhance the sensitivity of GC cells to platinum-based agents. Furthermore, the concurrent application of TIM1 knockdown and platinum chemotherapy exhibited synergistic anti-tumor effects.

The MAPK signaling pathway plays crucial roles in the processes of tumorigenesis, metastasis, angiogenesis, chemotherapy resistance, and immune responses [23, 32]. Wang *et al*. demonstrated that dual specificity phosphatase 5 pseudogene 1 modulates platinum sensitivity-based agents by mediating MAPK signaling [24]. Yu *et al*. also confirmed that the upregulation of ZXF1 contributes to cisplatin resistance by activating the MAPK pathway, which is correlated with unfavorable prognoses in cancer patients [33]. Furthermore, Li *et al*. reported that halofuginone enhances the sensitivity of lung cancer-like organ models to cisplatin by inhibiting MAPK signaling [34]. In this study, transcriptome sequencing and bioinformatic analysis were performed on GC cells from the shNC and sh2 groups, revealing that DEGs were most abundant and significantly altered within the MAPK signaling axis. This finding was corroborated by WB experiments, indicating that TIM1 may regulate GC cell biology through the MAPK signaling pathway.

Recent research has increasingly demonstrated a significant correlation between TIM1 expression and cancer patient prognosis. Zhou *et al*. reported that TIM1 expression is markedly elevated in glioma tissue compared with that in adjacent tissues, with patients exhibiting low TIM1 expression experiencing prolonged OS duration [35]. Additionally, TIM1 is highly expressed in cervical carcinoma but is nearly absent in normal cervical tissue [36]. Our investigation revealed that TIM1 is also highly expressed in GC tissues and is associated with the prognosis of GC patients. The Kaplan-Meier survival analysis revealed a negative correla-

tion between TIM1 expression and OS in these patients, suggesting that elevated TIM1 expression is predictive of poor survival outcomes in GC patients. Furthermore, we detected a significant increase in TIM1 expression in GC cell lines. Knockdown of TIM1 resulted in the inhibition of the proliferation, migration, and invasion of GC cells and slowed the growth rate of subcutaneous tumors. Zheng *et al*. reported that knockdown of TIM1 in NSCLC cell lines significantly impaired cell viability [16]. Chen *et al*. demonstrated that the upregulation of TIM1 enhanced the migration and invasion capabilities of CC cells while inhibiting their apoptosis [36]. TIM1 is also highly expressed in human glioma cells, and silencing TIM1 can impede cell proliferation, invasion, and migration [37]. These findings align with our conclusion that knockdown of TIM1 can decelerate the growth process of GC and suppress the malignant biologic characteristics of tumors. Consequently, the data indicate that TIM1 may play a role in promoting the initiation and progression of various tumors, including NSCLC, cervical cancer, glioma and gastric cancer.

Conclusion

TIM1 was identified as an oncogene in GC. Knockdown of TIM1 effectively improved platinum-based chemosensitivity and suppresses biological behaviors by the MAPK signaling pathway in GC. TIM1 may play a role in mediating resistance to chemotherapy and provide an underlying therapeutic strategy for enhancing chemotherapy. Consequently, TIM1 holds promise as a target for diagnosing and treating GC in clinical uses.

Acknowledgements

This work has benefited from databases above. We thank LetPub (www.letpub.com.cn) for its linguistic assistance during the preparation of this manuscript. This work was supported by the Natural Science Foundation of China (82472225, 32071223 and 32100729), Jiangxi Provincial Key Laboratory of Blood Transfusion (2024SSY06171), Medicine major science and technology R & D projects of Jiangxi Province (20213AAG01013), training plan for academic and technical leaders of major disciplines in Jiangxi Province (2021-3BCJ22015), Jiangxi Province Science and Technology Innovation Talent Project (jxsg-2023201037), science and technology innovation base plan of Jiangxi Province (20212BCD-42006), Graduate Innovative Special Fund Projects of Jiangxi Province (YC2021-B045 and YC2021-B057), Natural Science Foundation of Hubei Province (2025AFB275) and Guiding Project of Jingzhou Science and Technology Bureau (2024HD06 and 2024HD11). All participants in the study gave written informed consent.

Disclosure of conflict of interest

None.

Address correspondence to: Aiping Le, Department of Transfusion Medicine, Key Laboratory of Jiangxi Province for Transfusion Medicine, The First Affiliated Hospital, Jiangxi Medical College, Nanchang University, Nanchang, Jiangxi, P. R. China. E-mail: ndyfy00973@ncu.edu.cn

References

[1] Sung H, Ferlay J, Siegel RL, Laversanne M, Soerjomataram I, Jemal A and Bray F. Global cancer statistics 2020: GLOBOCAN estimates of incidence and mortality worldwide for 36 cancers in 185 countries. Ca Cancer J Clin 2021; 71: 209-249.

[2] Smyth EC, Nilsson M, Grabsch HI, van Grieken NC and Lordick F. Gastric cancer. Lancet 2020; 396: 635-648.

[3] Pilonis ND, Tischkowitz M, Fitzgerald RC and di Pietro M. Hereditary diffuse gastric cancer: approaches to screening, surveillance, and treatment. Annu Rev Med 2021; 72: 263-280.

[4] Hur H, Lee YJ, Kim YW, Min JS, Yoon HM, An JY, Eom BW, Cho GS, Park YK and Jung MR. Clinical efficacy of laparoscopic sentinel node navigation surgery for early gastric cancer: five-year results of SENORITA trial. J Clin Oncol 2022; 40: 4050.

[5] Rottenberg S, Disler C and Perego P. The rediscovery of platinum-based cancer therapy. Nat Rev Cancer 2021; 21: 37-50.

[6] Zhang C, Xu C, Gao X and Yao Q. Platinum-based drugs for cancer therapy and anti-tumor strategies. Theranostics 2022; 12: 2115-2132.

[7] Lv P, Man S, Xie L, Ma L and Gao W. Pathogenesis and therapeutic strategy in platinum resistance lung cancer. Biochim Biophys Acta Rev Cancer 2021; 1876: 188577.

[8] Arnesano F, Nardella MI and Natile G. Platinum drugs, copper transporters and copper chelators. Coord Chem Rev 2018; 374: 254-260.

[9] Xu Y, Han X, Li Y, Min H, Zhao X, Zhang Y, Qi Y, Shi J, Qi S, Bao Y and Nie G. Sulforaphane mediates glutathione depletion via polymeric nanoparticles to restore cisplatin chemosensitivity. ACS Nano 2019; 13: 13445-13455.
[10] Koren Carmi Y, Mahmoud H, Khamaisi H, Adawi R, Gopas J and Mahajna J. Flavonoids restore platinum drug sensitivity to ovarian carcinoma cells in a phospho-ERK1/2-dependent fashion. Int J Mol Sci 2020; 21: 6533.
[11] Wu J, Zhou Z, Li J, Liu H, Zhang H, Zhang J, Huang W, He Y, Zhu S, Huo M, Liu M and Zhang C. CHD4 promotes acquired chemoresistance and tumor progression by activating the MEK/ERK axis. Drug Resist Updat 2023; 66: 100913.
[12] Kuchroo VK, Umetsu DT, DeKruyff RH and Freeman GJ. The TIM gene family: emerging roles in immunity and disease. Nat Rev Immunol 2003; 3: 454-462.
[13] Wang J, Qiao L, Hou Z and Luo G. TIM-1 promotes hepatitis C virus cell attachment and infection. J Virol 2017; 91: e01583-16.
[14] Halim A, Bagley RG, Turner CD and Keler T. Prevalence and clinical implications of T-cell immunoglobulin mucin type-1 (TIM-1) in multiple tumor types. J Clin Oncol 2017; 35: 34.
[15] Nishikori M, Kishimoto W, Arima H, Shirakawa K, Kitawaki T and Takaori-Kondo A. Expression of Tim-1 and its pathogenetic role in primary CNS lymphoma. Blood 2014; 124: 2961.
[16] Zheng X, Xu K, Chen L, Zhou Y and Jiang J. Prognostic value of TIM-1 expression in human non-small-cell lung cancer. J Transl Med 2019; 17: 178.
[17] Liu L, Song Z, Zhao Y, Li C, Wei H, Ma J and Du Y. HAVCR1 expression might be a novel prognostic factor for gastric cancer. PLoS One 2018; 13: e0206423.
[18] Xue J, Li Y, Yi J and Jiang H. HAVCR1 affects the MEK/ERK pathway in gastric adenocarcinomas and influences tumor progression and patient outcome. Gastroenterol Res Pract 2019; 2019: 6746970.
[19] Oun R, Moussa YE and Wheate NJ. The side effects of platinum-based chemotherapy drugs: a review for chemists. Dalton Trans 2018; 47: 6645-6653.
[20] Flores-Romero H, Hohorst L, John M, Albert MC, King LE, Beckmann L, Szabo T, Hertlein V, Luo X, Villunger A, Frenzel LP, Kashkar H and Garcia-Saez AJ. BCL-2-family protein tBID can act as a BAX-like effector of apoptosis. EMBO J 2022; 41: e108690.
[21] Lopez A, Reyna DE, Gitego N, Kopp F, Zhou H, Miranda-Roman MA, Nordstrøm LU, Narayanagari SR, Chi P, Vilar E, Tsirigos A and Gavathiotis E. Co-targeting of BAX and BCL-XL proteins broadly overcomes resistance to apoptosis in cancer. Nat Commun 2022; 13: 1199.
[22] Ronkina N and Gaestel M. MAPK-activated protein kinases: servant or partner? Annu Rev Biochem 2022; 91: 505-540.
[23] Anjum J, Mitra S, Das R, Alam R, Mojumder A, Emran TB, Islam F, Rauf A, Hossain MJ, Aljohani ASM, Abdulmonem WA, Alsharif KF, Alzahrani KJ and Khan H. A renewed concept on the MAPK signaling pathway in cancers: polyphenols as a choice of therapeutics. Pharmacol Res 2022; 184: 106398.
[24] Wang X, Zhang L, Liang Q, Wong CC, Chen H, Gou H, Dong Y, Liu W, Li Z, Ji J and Yu J. DUSP5P1 promotes gastric cancer metastasis and platinum drug resistance. Oncogenesis 2022; 11: 66.
[25] Uxa S, Castillo-Binder P, Kohler R, Stangner K, Müller GA and Engeland K. Ki-67 gene expression. Cell Death Differ 2021; 28: 3357-3370.
[26] Sexton RE, Al Hallak MN, Diab M and Azmi AS. Gastric cancer: a comprehensive review of current and future treatment strategies. Cancer Metastasis Rev 2020; 39: 1179-1203.
[27] Bian G, Li W, Huang D, Zhang Q, Ding X, Zang X, Ye Y, Cao J and Li P. The cancer/testis antigen HORMAD1 promotes gastric cancer progression by activating the NF-κB signaling pathway and inducing epithelial-mesenchymal transition. Am J Transl Res 2023; 15: 5808-5825.
[28] Nakasuka F, Hirayama A, Makinoshima H, Yano S, Soga T and Tabata S. The role of cytidine 5'-triphosphate synthetase 1 in metabolic rewiring during epithelial-to-mesenchymal transition in non-small-cell lung cancer. FEBS Open Bio 2024; 14: 1570-1583.
[29] Lai CY, Lee C, Yeh TS, Chang ML, Lin YS and Chen TH. Peripheral blood inflammatory markers as a reliable predictor of gastric mucosal metaplasia change in the middle-aged population. J Cancer 2024; 15: 3313-3320.
[30] Huang Z, Dong J, Guo T, Jiang W, Hu R, Zhang S, Du T and Jiang X. TRIM28 regulates proliferation of gastric cancer cells partly through SRF/IDO1 axis. J Cancer 2024; 15: 4417-4429.
[31] Du P, Xiong R, Li X and Jiang J. Immune regulation and antitumor effect of TIM-1. J Immunol Res 2016; 2016: 8605134.
[32] Xu Y, Sun Q, Yuan F, Dong H, Zhang H, Geng R, Qi Y, Xiong X, Chen Q and Liu B. RND2 attenuates apoptosis and autophagy in glioblastoma cells by targeting the p38 MAPK signalling pathway. J Exp Clin Cancer Res 2020; 39: 174.
[33] Yu T, Bai W, Su Y, Wang Y, Wang M and Ling C. Enhanced expression of lncRNA ZXF1 promotes cisplatin resistance in lung cancer cell via MAPK axis. Exp Mol Pathol 2020; 116: 104484.

[34] Li H, Zhang Y, Lan X, Yu J, Yang C, Sun Z, Kang P, Han Y and Yu D. Halofuginone sensitizes lung cancer organoids to cisplatin via suppressing PI3K/AKT and MAPK signaling pathways. Front Cell Dev Biol 2021; 9: 773048.

[35] Zhou P, Fei M, Han Y, Zhou M and Wang H. Knockdown of T cell immunoglobulin and mucin 1 (Tim-1) suppresses glioma progression through inhibition of the cytokine-PI3K/AKT pathway. Onco Targets Ther 2020; 13: 7433-7445.

[36] Chen L, Qing J, Xiao Y, Huang X, Chi Y and Chen Z. TIM-1 promotes proliferation and metastasis, and inhibits apoptosis, in cervical cancer through the PI3K/AKT/p53 pathway. BMC Cancer 2022; 22: 370.

[37] Wei L, Peng Y, Shao N and Zhou P. Downregulation of Tim-1 inhibits the proliferation, migration and invasion of glioblastoma cells via the miR-133a/TGFBR1 axis and the restriction of Wnt/β-catenin pathway. Cancer Cell Int 2021; 21: 347.

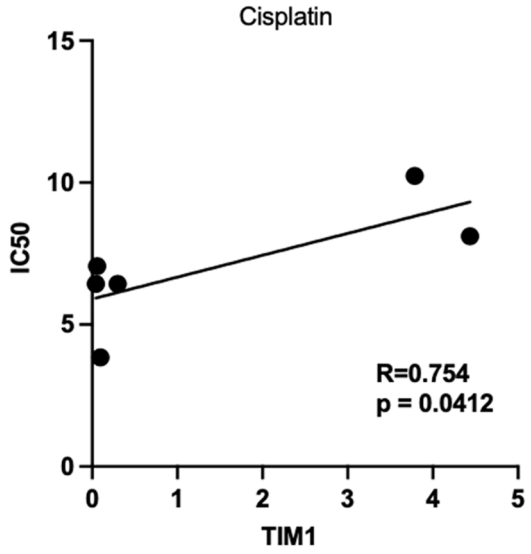

Figure S1. The correlation between the IC_{50} of platinum drug (cisplatin) and the TIM1 expression in GC cell lines by the Genomics of Drug Sensitivity in Cancer database.

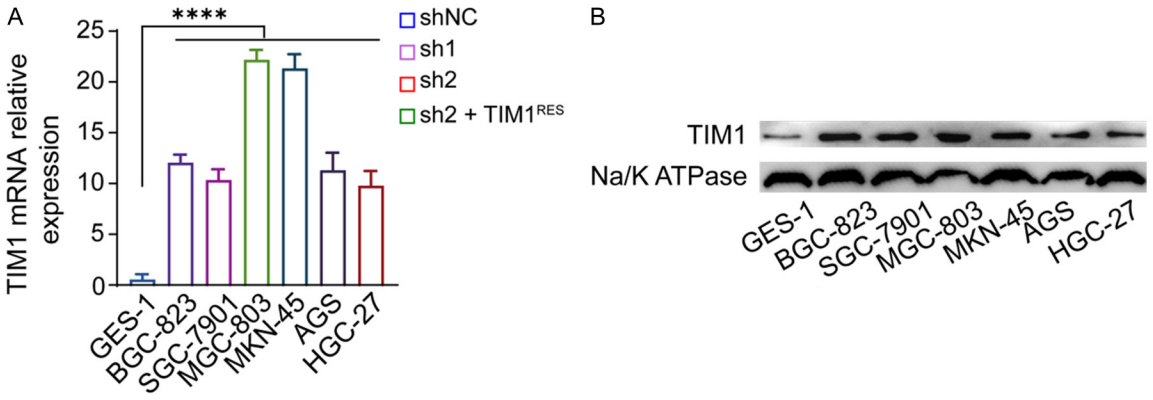

Figure S2. Expression levels of TIM1 in gastric epithelial cells and GC cell lines. a,b: qRT-PCR (A) and WB (B) detection of TIM1 expression level in gastric epithelial cells (GES-1) and GC cell lines. Data are shown as mean ± SD. ****P < 0.0001.

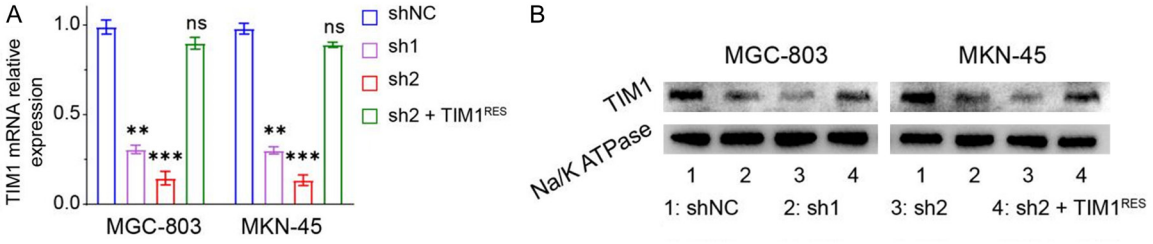

Figure S3. Expression levels of TIM1 in shNC, TIM1 knockdown and $TIM1^{RES}$. (A, B) Levels of TIM1 were assessed in shNC, TIM1 knockdown (sh1 and sh2) and $TIM1^{RES}$ by qRT-PCR (A) and WB (B). Data are shown as mean ± SD. **P < 0.01, and ***P < 0.001.

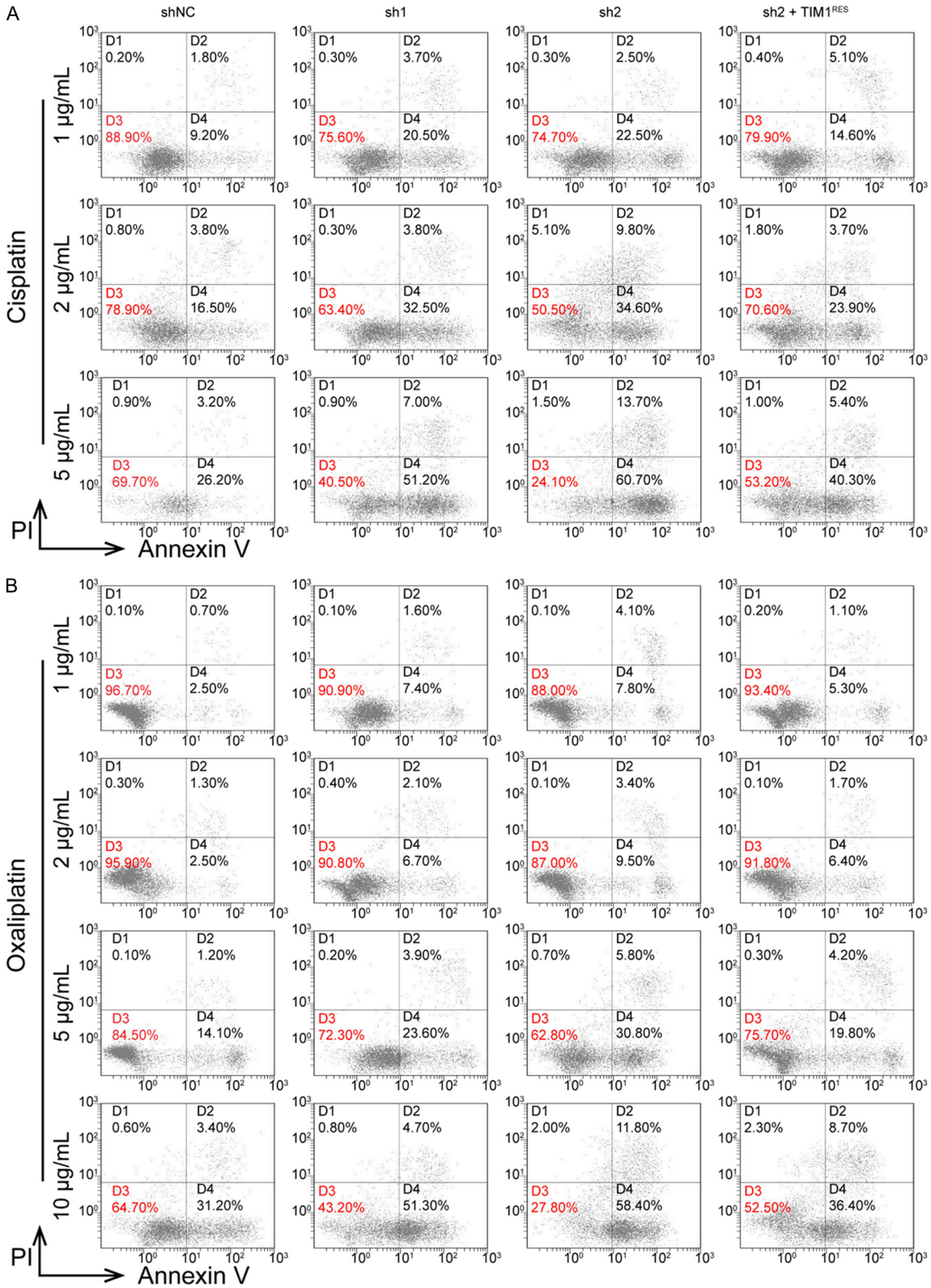

Figure S4. Knockdown of TIM1 enhanced the sensitivity of MGC-803 cells to platinum chemotherapeutic drugs. (A, B) After 48 h of treatment with different concentrations of cisplatin (A) and oxaliplatin (B), the apoptosis of MGC-803 cells in each group was detected by flow cytometry.

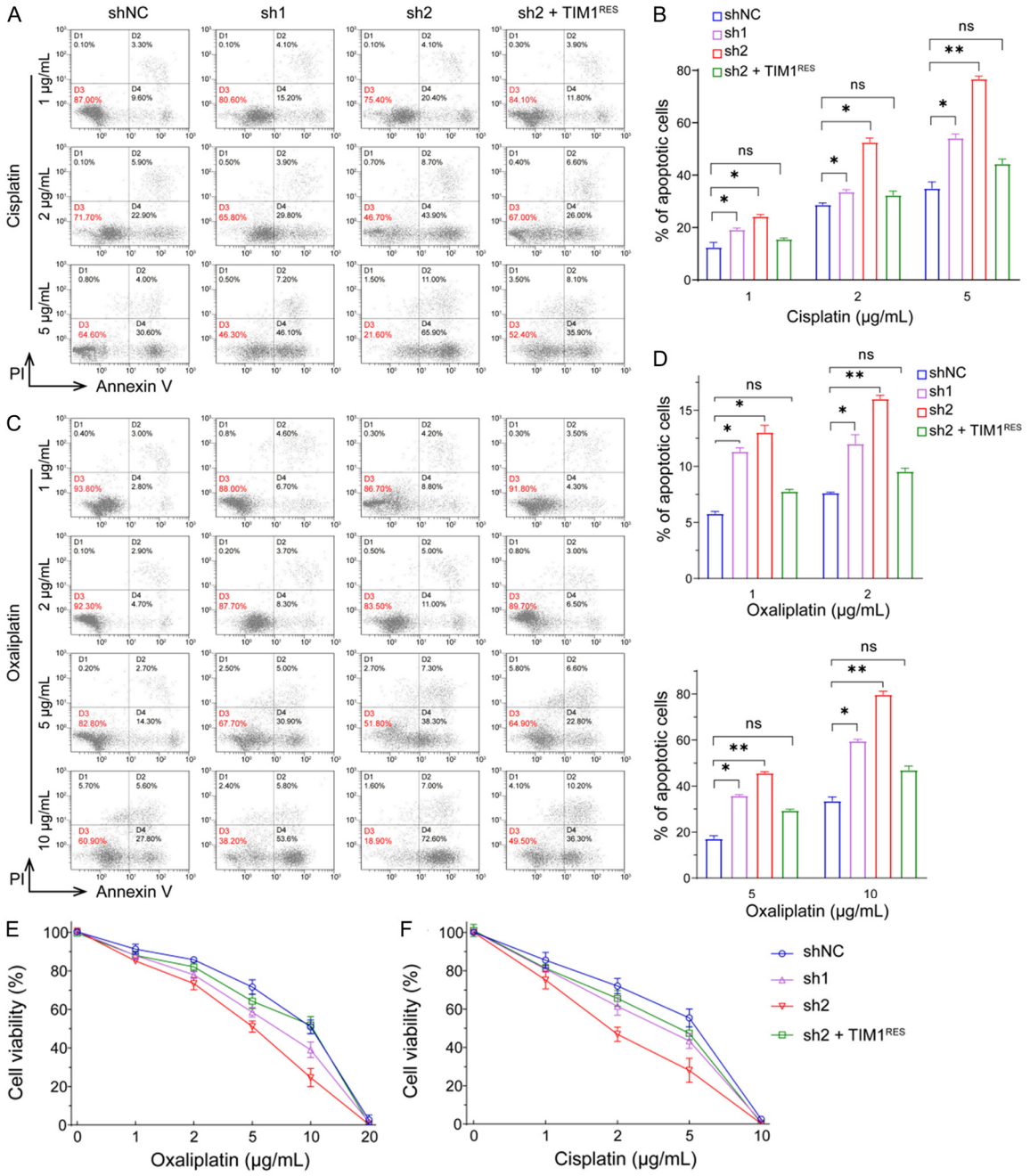

Figure S5. Knockdown of TIM1 enhanced the sensitivity of MKN-45 cells to platinum chemotherapeutic drugs. (A, B) After 48 h of treatment with different concentrations of cisplatin, the apoptosis of MKN-45 cells in each group was detected by flow cytometry (A) and the histograms of the corresponding results from each group apoptotic cells (B). (C, D) After 48 h of treatment with different concentrations of oxaliplatin, the apoptosis of MKN-45 cells in each group was detected by flow cytometry (C) and bar charts showed the percentage of apoptotic cells in each group (D). (E, F) After 48 h of treatment with different concentrations of cisplatin (E) and oxaliplatin (F), the cell viability of MKN-45 cells was assessed by CCK8 assay. Data were shown as mean ± SD.*$P < 0.05$, **$P < 0.01$, and ns (not significant).

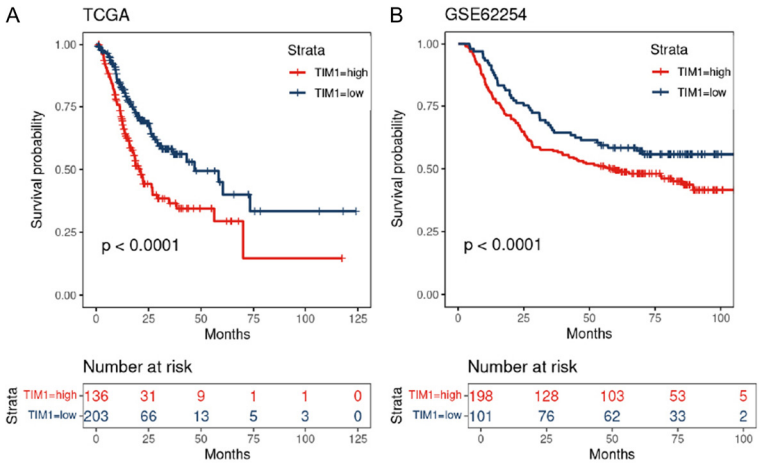

Figure S6. Correlation between TIM1 expression level and survival prognosis of GC patients in the TCGA database (A) and GSE62254 database (B).

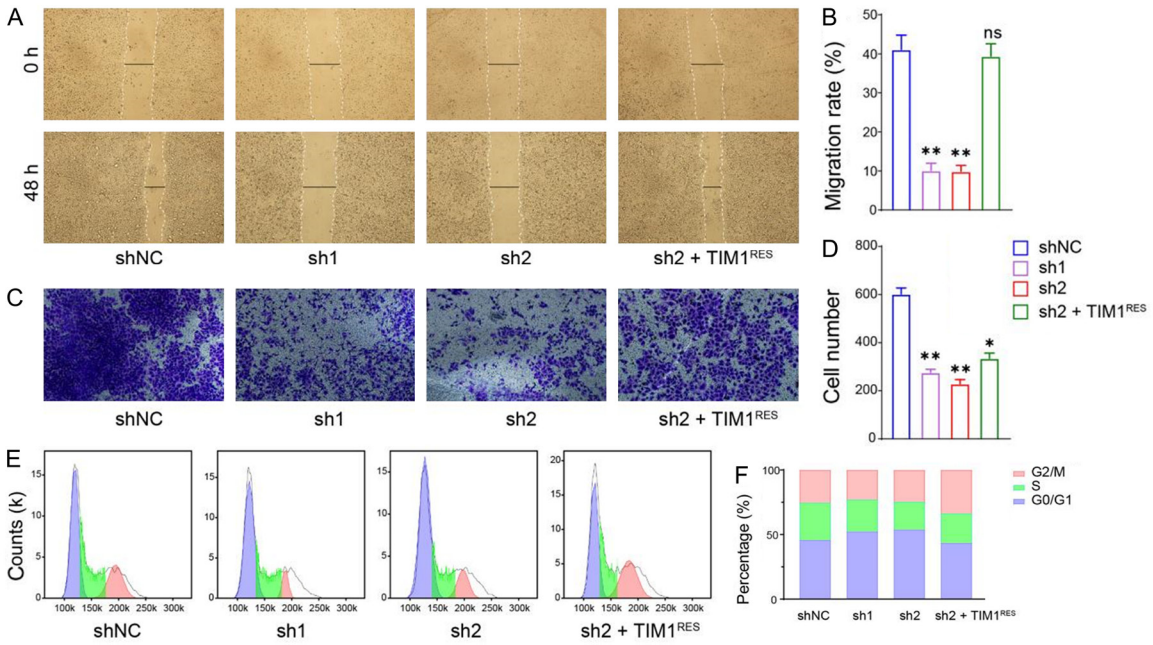

Figure S7. Knockdown of TIM1 inhibited the malignant biologic behavior of GC cells *in vitro*. (A) Cell migration ability of MKN-45 with shNC, TIM1 knockdown, and TIM1^{RES} detected by scratch assay. (B) Bar charts showed the percentage of migration rate in each group of MKN-45 cells. (C, D) Representative images of MKN-45 cells transwell invasion assay in each group (C) and quantification the number of invaded cells in each group (D). (E) Flow cytometry was performed to detect cell cycle of MKN-45 cells in each group. (F) The percentages of MKN-45 cells in the different cycle phases are shown in (F). Data are shown as mean ± SD.*P < 0.05, **P < 0.01, and ns (not significant).